ACS Energy LETTERS

http://pubs.acs.org/journal/aelccp

Interfacial Dipole Layer Enables High-Performance Heterojunctions for Photoelectrochemical Water Splitting

Juwon Yun, Jeiwan Tan, Young-Kwang Jung, Wooseok Yang, Hyungsoo Lee, Sunihl Ma, Young Sun Park, Chan Uk Lee, Wenzhe Niu, Jeongyoub Lee, Kyungmin Kim, S. David Tilley, Aron Walsh,* and Jooho Moon*

Cite This: *ACS Energy Lett.* 2022, 7, 1392−1402

Read Online

ACCESS | Metrics & More | Article Recommendations | Supporting Information

ABSTRACT: **TiO_2 has been widely used as an n-type overlayer, simultaneously serving as a protective layer for photocathodes. However, the photovoltage generated from a TiO_2 junction with p-type absorbers, such as p-Si, Sb_2Se_3, SnS, and Cu_2O, is insufficient. We report a dipole reorientation strategy to overcome this limitation by inserting a polyethylenimine ethoxylated (PEIE) layer between a p-type absorber and TiO_2. Furthermore, we demonstrate that the PEIE dipole orientation can be rearranged by increasing the layer thickness, leading to an upward shift of the TiO_2 band edge. The magnitude of band shift induced by the dipole effect depends on the TiO_2 layer thickness. Using this approach, the onset potential was significantly improved to 0.5 V versus the reversible hydrogen electrode (V_{RHE}) in a p-Si/PEIE/TiO_2/Pt device. The versatility of the effective dipole reorientation strategy was demonstrated by application to a range of TiO_2-protected heterojunction photocathodes based on Sb_2Se_3, Cu_2O, and SnS.**

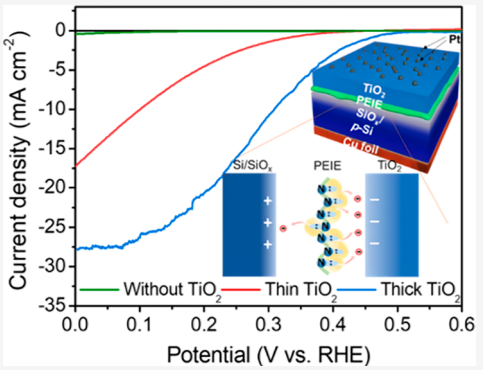

Photoelectrochemical (PEC) water splitting has attracted significant attention because it can directly convert sustainable solar energy to hydrogen.[1] A high solar-to-hydrogen (STH) efficiency of a bias-free device should be achieved to practically use eco-friendly and sustainable hydrogen energy. Light-absorbing semiconductors must generate a sufficient photovoltage for unbiased solar water splitting to exceed the thermodynamic barrier of water splitting (1.23 V) and overpotential for electrochemical reactions at the surface while compensating potential losses for charge recombination.[2,3] Maximizing the quasi-Fermi level difference at the interface is crucial for implementing highly efficient and bias-free solar water splitting, because the photovoltage of a semiconductor is determined by the quasi-Fermi level difference of electrons and holes at the interface under illumination.[4] Generally, most p-type semiconductor-based photocathodes have a junction with an n-type layer to generate an additional photovoltage for efficient carrier separation.[5] Among many n-type candidates, TiO_2 is most widely used as a physical protector due to its superior chemical stability over a wide range of pH.[6] However, the photovoltage from the TiO_2-protected heterojunction p-type photocathodes (TPHPs), including Si, Sb_2Se_3, SnS, and Cu_2O, is still insufficient due to unfavorable band alignment.[7−10]

Various band alignment engineering strategies, such as specific treatment and insertion of a functional material, have been attempted to tune the band alignment between the p-type materials and n-type TiO_2-protection layer to obtain a high photovoltage from the TPHP.[3,4,11] For instance, the surface n^+ doping by phosphorus diffusion process creates an additional buried p−n junction through which the Fermi level of p-Si shifts upward, leading to an enlarged quasi-Fermi level difference and an improved photovoltage.[12−14] However, the n^+-doping process requires a highly complicated and toxic process.[13] Inserting a Ga_2O_3 buffer layer at the interface of Cu_2O and TiO_2 can also generate high photovoltage by minimizing the conduction band offset.[9] It has also been reported that CdS can be utilized as a buffer layer for Sb_2Se_3 to reduce the valence band mismatch, improving the photovoltage.[8,15] However, the buffer layer insertion may not be

Received: February 18, 2022
Accepted: March 18, 2022

https://doi.org/10.1021/acsenergylett.2c00392
ACS Energy Lett. 2022, 7, 1392−1402

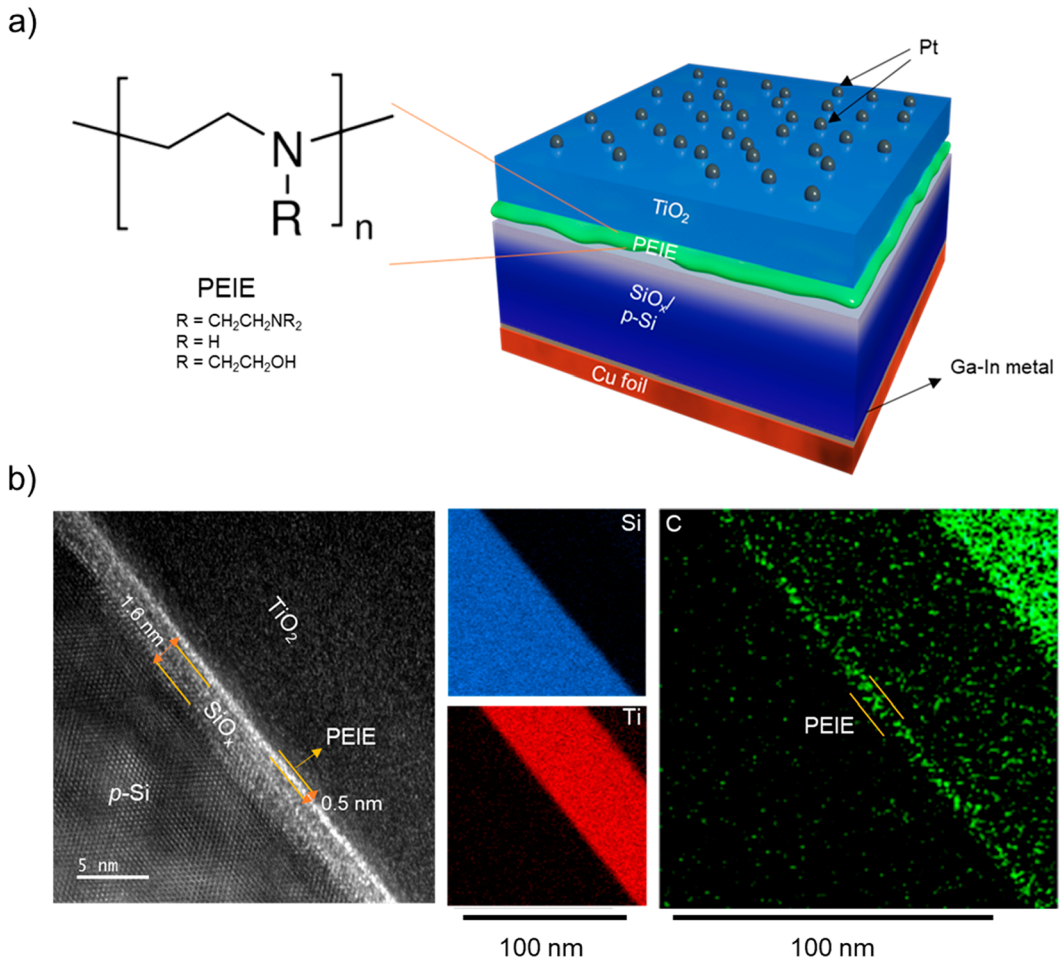

Figure 1. (a) Device structure of photocathodes in a Cu foil/Ga−In metal/p-Si/SiO_x/PEIE/TiO_2/Pt configuration. (b) High-magnification TEM image and EDS elemental mapping images of the p-Si/PEIE/TiO_2 structure.

generically exploitable because this strategy only works under a specific material combination with proper band energy positions (e.g., Ga_2O_3 for Cu_2O/TiO_2 TPHP and CdS for Sb_2Se_3/TiO_2 TPHP).

Diverse dipolar molecules have been introduced at the heterojunction interface as an alternative to a buffer layer to develop an interfacial dipole moment by either charge rearrangement or transfer.[16,17] The net interfacial dipole moment induces an internal electric field altering the band bending, effectively tuning the band energy alignment at the equilibrium state.[16,18] The direction of the band shift is related to an orientation of the net dipole moment at the interface in which the adsorption of negative dipole molecules leads to an upward shift of the band edge; however, the presence of positive dipole molecules lowers the band position.[16−21] The influence of the dipole strategy is generally highly dependent on the thickness of the dipole layer and neighboring layers because the net interfacial dipole moment is proportional to the magnitude of polarization that depends on the thicknesses of both the dipole molecule and adjacent layers.[7,22,23] The dipole strategies in a photocathode have been suggested to lower the band edge of the absorber layer by locating the positive dipole molecules on the p-type semiconductor to enlarge the band bending with respect to the water redox potential or TiO_2 layer.[7,19−21] However, the conventional dipole strategy (i.e., tuning the band edge of p-type semiconductor) inevitably induces a limited dipole effect because the thickness of the absorbing layer is predetermined for the light-harvesting and carrier diffusion distances. Therefore, the effect of the dipole strategy cannot be fully exploited. The dipole strategy has been successfully applied to p-Si; however, the adsorption of a positive dipole molecule on other semiconductors, such as Sb_2Se_3 and Cu_2O thin films, shows a less significant effect.[7] Hence, it is highly demanding to develop a simple and universally applicable dipole strategy enabling high-performance TPHP with high photovoltage.

This study proposes a dipole reorientation strategy by controlling TiO_2 thickness. Polyethylenimine ethoxylate (PEIE) was introduced as a negative dipole molecule into a Si-based TPHP (i.e., p-Si/PEIE/TiO_2/Pt).[16,24,25] PEIE has been widely utilized to lower the work functions of metals and metal oxides in photovoltaics.[26−28] However, the thickness of adjacent layers has rarely been considered to control the PEIE dipole orientation. In the Si-based TPHP structure, the amine groups in PEIE induce strong electrostatic interaction with TiO_2 upon an increased TiO_2 thickness due to its high polarizability, which in turn results in dipole reorientation and upward shift of TiO_2 band edge.[25] We suggest the mechanism for the photovoltage improvement on the basis of a combination of experimental observations and theoretical calculations. The photovoltage was significantly enhanced by controlling the TiO_2-thickness-dependent dipole effect, which improved the onset potential to 0.5 V versus the reversible hydrogen electrode (V_{RHE}) in the p-Si/PEIE/TiO_2/Pt device.

https://doi.org/10.1021/acsenergylett.2c00392
ACS Energy Lett. 2022, 7, 1392−1402

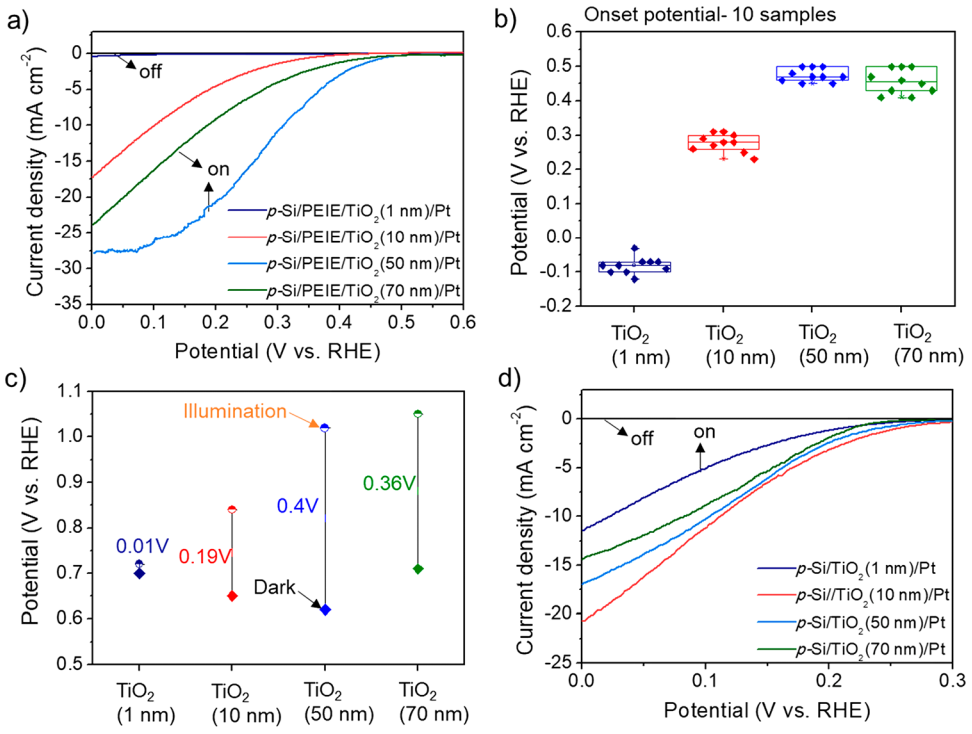

Figure 2. (a) LSV curves and (b) device performance statistics of the onset potential obtained from 10 cells of p-Si/PEIE(0.025 wt %)/TiO_2/Pt photocathodes with different TiO_2 thicknesses (i.e., 1, 10, 50, and 70 nm) under 1 sun illumination in a H_2SO_4 electrolyte (pH 1). (c) Open-circuit voltage (OCV) of PEIE-modified Si photocathodes with different TiO_2 thicknesses (i.e., 1, 10, 50, and 70 nm) under 1 sun illumination with argon purging. (d) LSV curves of p-Si/TiO_2/Pt photocathodes with different TiO_2 thicknesses (i.e., 1, 10, 50, and 70 nm) under 1 sun illumination in a H_2SO_4 electrolyte (pH 1).

Furthermore, we demonstrate that the PEIE dipole reorientation strategy is readily applicable to other semiconductor-based TPHPs, such as Sb_2Se_3, SnS, and Cu_2O, leading to an improved onset potential. Our study provides a simple and synergistic dipole effect of PEIE and TiO_2 to improve the photovoltage of TiO_2-protected heterojunction p-type photocathodes for PEC water splitting.

We introduced a PEIE layer at the interface between p-Si/SiO_x and TiO_2/Pt to fabricate a PEIE-modified p-Si-based photocathode, as schematically shown in Figure 1a. A surface-cleaned p-type Si wafer was dipped into a PEIE aqueous solution (typically at a concentration of 0.025 wt %) for 20 min, followed by N_2 blowing and immediate deposition of TiO_2 by ALD. Sputtered Pt was employed as a cocatalyst, while Ga−In alloy and Cu foil were used as back contacts to support a full device (see the Experimental Section in the Supporting Information for further details). X-ray diffraction (XRD) patterns exhibited identical peaks regardless of PEIE deposition, suggesting that PEIE does not alter the crystallinity of Si (Figure S1). Scanning transmission electron microscopy (STEM) and energy-dispersive X-ray spectroscopy (EDS) were performed onto the cross-sectioned device by a focused ion beam (FIB) to obtain direct evidence for the existence of the PEIE layer (Figure 1b). The C signal in the right upper corner in Figure 1b did not result from PEIE. It is speculated that the significant C signal can be attributed to the adsorbed carbon atoms from the ambient atmosphere. Furthermore, it can be seen from EDX mapping that there was no inward diffusion of Ti metal into the p-Si during the ALD process. The analysis confirmed the existence of carbon elements at the p-Si/TiO_2 interface with a thickness of ∼0.5 nm, which is thinner than the native oxide layer (i.e., SiO_x ∼1.6 nm) inevitably formed during the PEIE deposition despite the etching. We denote p-Si/SiO_x as "p-Si," including the native oxide layer, for convenience. The thickness of PEIE on p-Si was evaluated using ellipsometry, from which the PEIE layer obtained from a 0.025 wt % solution had a thickness of ∼0.55 ± 0.23 nm, matching well with the value measured by a STEM-EDS analysis.

Interestingly, the champion PEC performance of PEIE-modified p-Si photocathodes characterized by linear sweep voltammetry (LSV) under 1 sun illumination varied depending on the TiO_2 overlayer thickness, as verified by ellipsometry measurements (Figure 2a and Figure S2). Ultrathin TiO_2 (∼1 nm) was deposited on the PEIE to prevent electrolyte penetration, due to the instability of PEIE in an acidic environment.[20,24] We observed low performance in the p-Si/PEIE/TiO_2(1 nm)/Pt sample, showing a value of 0.5 mA cm^{-2} at 0 V_{RHE}; however, the current density was 17 mA cm^{-2} at 0 V_{RHE} with a TiO_2 thickness of 10 nm. The performance of the PEIE-modified device was maximized at a thickness of ∼50 nm, whereas the current density in the 0.2−0.4 V_{RHE} range was significantly decreased when TiO_2 became thicker than 50 nm. The LSV curves were linearly extrapolated at 1 mA cm^{-2} toward a rapidly increasing region where the photocurrent mainly contributed to the hydrogen evolution reaction (HER), excluding the non-Faradaic current, to determine the onset potential of the photocathodes (Figure S3).[3] The onset potential changed with increasing TiO_2 thickness from a negative potential of −0.05 V_{RHE} (at TiO_2 ∼1 nm) to a positive potential of 0.32 V_{RHE} (at TiO_2 ∼10 nm), reaching a more positive potential of 0.50 V_{RHE} (at TiO_2 ∼50 nm) and maintaining the similar slopes of LSV curves at 1 mA cm^{-2}. However, the potential slightly decreased to 0.47 V_{RHE} for the

https://doi.org/10.1021/acsenergylett.2c00392
ACS Energy Lett. 2022, 7, 1392−1402

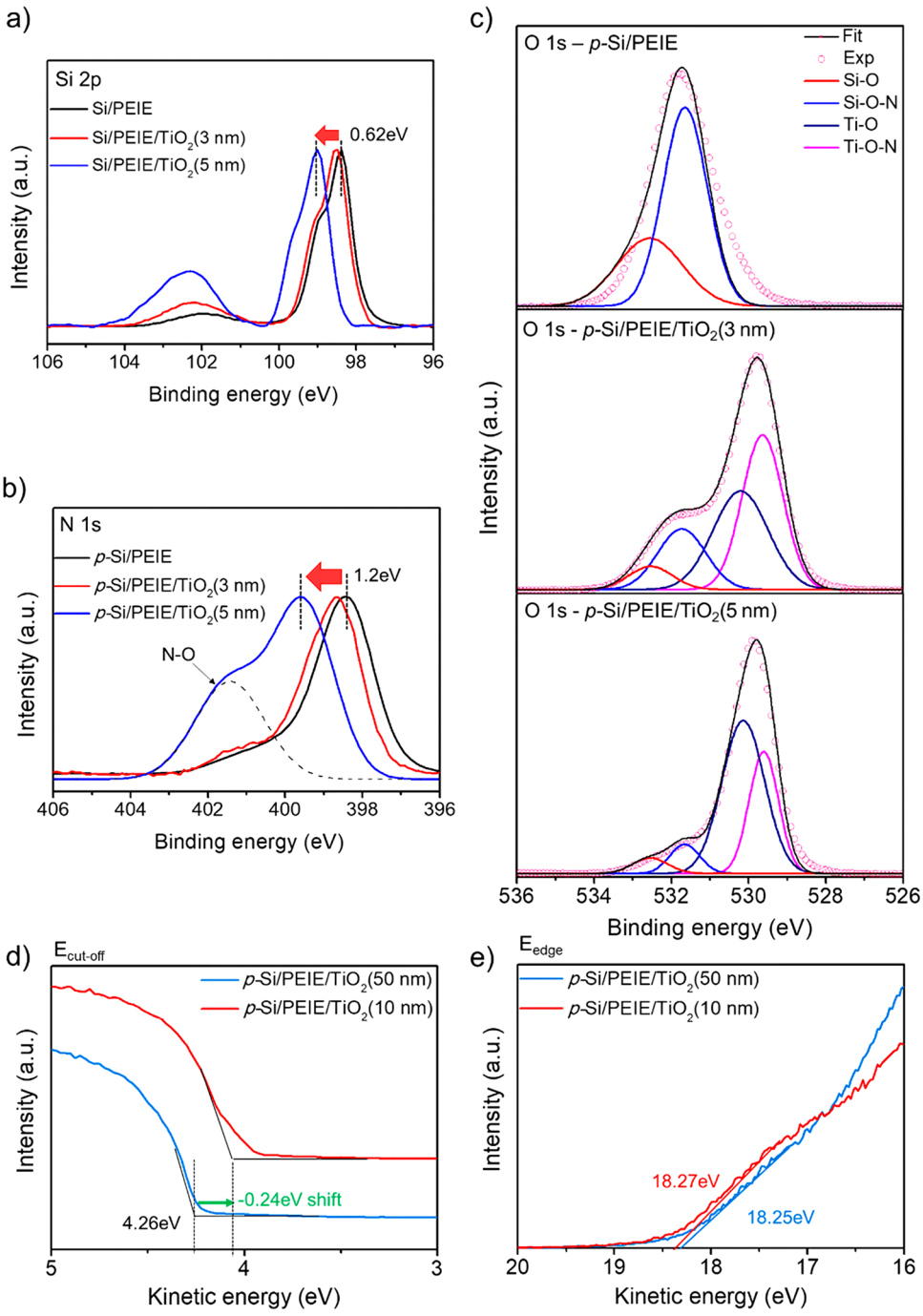

Figure 3. XPS spectra of (a) Si 2p and (b) N 1s and (c) deconvolution of O 1s regions before and after TiO_2 deposition (3 and 5 nm). Scatter points represent the original experimental data, whereas solid lines represent the fitted curves. Normalized UPS spectra of (d) the secondary electron cutoff region and (e) the valence band edge for p-Si/PEIE/TiO_2(10 and 50 nm).

70 nm thick TiO_2. Furthermore, the statistics of the onset potential obtained from the LSV curve for 10 separately fabricated samples confirmed the reproducibility of our PEIE-modification strategy (Figure 2b). The average onset potentials with a narrow deviation were −0.08, 0.28, 0.48, and 0.46 V_{RHE} at TiO_2 thicknesses of 1, 10, 50, and 70 nm, respectively. The negative onset potential (from −0.05 to −0.08 V_{RHE}) for p-Si/PEIE/TiO_2(1 nm)/Pt indicates that PEIE provides a negative dipole layer onto p-Si, leading to upward shifting of the band energy and less band bending with respect to the water redox potential.[18,19,29] However, the onset potential gradually shifted toward a positive potential accompanied by a performance enhancement with an increasing thickness of TiO_2. This is an unusual observation with respect to previous relevant reports.

We determined the open-circuit photovoltage (OCP) to gain an in-depth understanding of the variation in the onset potential depending on TiO_2 thickness; it is frequently used to reveal the photovoltage enhancement proportionally. The OCP, defined as the difference between open-circuit voltage (OCV) under illumination and in the dark (i.e., OCP = OCV_{light} − OCV_{dark}; also known as the resting potential), represents the degree of the band bending at the time of illumination with respect to the dark condition flattening the band bending in the depletion region.[30] Figure 2c shows that

https://doi.org/10.1021/acsenergylett.2c00392
ACS Energy Lett. 2022, 7, 1392−1402

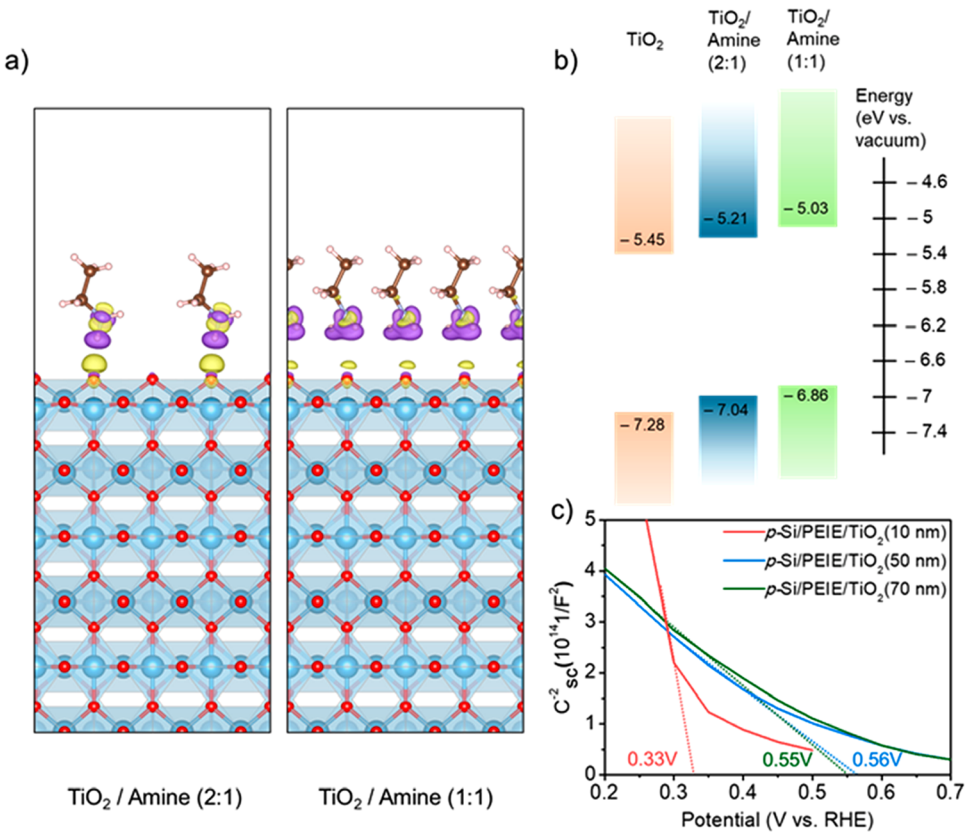

Figure 4. (a) Optimized configuration that magnified one side of the slab model and (b) energy band calculation of TiO_2/amine with different coverage ratios. (c) Capacitance (C_{sc}) variation with the applied potential presented in the Mott−Schottky relationship for p-Si/PEIE/TiO_2 photocathodes with different TiO_2 thicknesses (10, 50, and 70 nm) in the dark.

the OCP is 0.01, 0.19, 0.4, and 0.36 V at TiO_2 thicknesses of 1, 10, 50, and 70 nm in p-Si/PEIE/TiO_2/Pt, respectively. The higher OCP value indicates a more favorable driving force for water reduction, as determined by the larger difference between the electron quasi-Fermi levels of p-Si and TiO_2.[31] In the dark, there were approximately 600−700 mV deviations of the OCV value (i.e., OCV_{dark}) from 0 V vs RHE, which was commonly observed in all PEIE-modified Si photocathodes regardless of the TiO_2 thickness under diverse atmospheres (H_2, argon, and O_2) (Figure S4). We presume that the surface states of the amorphous TiO_2 layer cause a Fermi level pinning at the TiO_2/electrolyte in the dark.[31,32] The OCP measurement clearly confirmed that the photovoltage developed by p-Si/PEIE/TiO_2/Pt is dependent on the TiO_2 thickness. To further confirm the onset potential variation as a function of TiO_2 thickness in the absence of PEIE, we observed the performance of p-Si photocathodes with different TiO_2 thicknesses under 1 sun illumination (Figure 2d). The onset potentials were nearly identical regardless of TiO_2 thickness without the PEIE dipole layer, and the TiO_2 thickness less significantly affected the photocurrent density of the Si photocathode in comparison with the PEIE-modified Si photocathode. The morphologies of TiO_2 and PEIE/TiO_2 were observed by scanning electron microscopy (SEM) and atomic force microscopy (AFM) (Figure S5). It was confirmed that both layers revealed nearly identical morphologies and surface roughnesses. The presence of a PEIE dipole layer was unable to alter the morphology of overlying TiO_2. Therefore, it can be inferred that the PEIE dipole layer may interact electrostatically with TiO_2.

X-ray photoelectron spectroscopy (XPS) was used to understand the electronic states at the interface between p-Si and TiO_2 with the PEIE dipole layer. We analyzed three samples with varying TiO_2 thicknesses considering the average penetration depth of XPS analysis, p-Si/PEIE without TiO_2, p-Si/PEIE/TiO_2 (3 nm), and p-Si/PEIE/TiO_2 (5 nm), to elucidate the electrostatic interaction with PEIE. Figure 3a shows the Si 2p XPS spectra based on the TiO_2 thickness. The Si peak was located at 98.4 eV in the p-Si/PEIE without TiO_2 sample; the negative shift by 0.7 eV is attributed to negative dipoles developed by PEIE rather than the peak of bare Si (i.e., 99.1 eV) (Figure S6a).[29] However, the Si peak shifted to higher binding energy after TiO_2 deposition, suggesting that the previously formed electrostatic interaction of p-Si with PEIE weakens in the presence of TiO_2. Figure 3b shows the N 1s XPS spectra. It reveals the interaction variation of amine groups in PEIE on the basis of the TiO_2 thickness, in which the N 1s peak is shifted toward higher binding energy; however, Ti peaks for both p-Si/PEIE/TiO_2(3 nm) and p-Si/PEIE/TiO_2(5 nm) changed to lower binding energy in comparison to bare TiO_2 in Ti 2p XPS spectra (Figure S6b).[33] It can be inferred that more electrons from the amine are transferred to the TiO_2 side instead of to p-Si, as indicated by an intensified N−O interaction, leading to strong electrostatic interactions with TiO_2 after an increase in thickness.[33,34] O 1s XPS spectra (Figure 3c) showed a new peak related to TiO_2 at approximately 530 eV; the previous peak of p-Si/PEIE without TiO_2 appeared as a shoulder in p-Si/PEIE/TiO_2(3 and 5 nm). The broad peaks at 532.5 and 531.7 eV are assigned to Si−O and Si−O−N interactions in the p-Si/PEIE without TiO_2

https://doi.org/10.1021/acsenergylett.2c00392
ACS Energy Lett. 2022, 7, 1392−1402

sample. However, the newly emerged peaks at 530.2 and 529.6 eV are ascribed to Ti−O and Ti−O−N in the p-Si/PEIE/TiO_2(3 and 5 nm) samples.[35−38] The relative fraction of peak area of Si−O−N in the p-Si/PEIE without TiO_2 sample was 2-fold larger than that of Si−O (Table S1). The p-Si/PEIE/TiO_2(3 nm) sample showed that the peak area fraction of Ti−O−N (0.4) was 2 times larger than that of Si−O−N (0.19), implying that PEIE forms more electrostatic interactions with TiO_2 than with p-Si. The peak area fraction of Si−O−N decreased significantly to 0.07 with an increasing thickness of TiO_2; however, the peak area fraction of Ti−O−N was found to be 4-fold larger than that of Si−O−N. The increased peak portion of Ti−O−N with respect to Si−O−N also suggests that PEIE preferably forms more electrostatic interactions with an increasing thickness of TiO_2 than it does with p-Si. Therefore, we conclude that the the electrostatic interaction between p-Si and amine weakens with an increasing TiO_2 thickness, whereas more amine groups of PEIE are attracted toward the neighboring TiO_2 to form strong electrostatic interactions.

We performed ultraviolet photoelectron spectroscopy (UPS) measurements to clarify the dipole direction variation at the p-Si/PEIE interface in the presence of TiO_2.[16] The thickness of TiO_2 on p-Si/PEIE was controlled to ∼10 nm to gain access to the buried interface of PEIE/TiO_2 while avoiding the detection of the p-Si work function of the substrate, due to an approximate information depth of around 10 nm from UPS. The p-Si/PEIE/TiO_2 (50 nm) sample was employed as a reference, as it had a relatively thick TiO_2 overlayer. The work function of p-Si/PEIE/TiO_2(10 nm) determined by a linear extrapolation of the kinetic energy at the cutoff region was decreased to 4.02 eV in comparison with p-Si/PEIE/TiO_2 (50 nm) (4.26 eV) (Figure 3d). This result indicates that the vacuum level for the PEIE/TiO_2 interface shifts downward.[39,40] Figure 3e shows the valence band region of each sample, revealing a feature similar to that of pristine TiO_2 (Figure S7); it shows that the feature related to the p-Si substrate is not as observable as would be expected. Additionally, the UPS result of the p-Si/PEIE interface revealed a decrease in work function by 0.56 eV without the TiO_2 layer, suggesting that PEIE develops a negative dipole on the p-Si (Figure S8).[16,24] Consequently, we conclude that PEIE induces a negative dipole to p-Si prior to TiO_2 deposition; however, a net dipole moment of PEIE is reoriented by inducing the negative charges to the adjacent TiO_2 after TiO_2 deposition (Figure S9).[39−41]

Density functional theory (DFT) simulations were performed to further understand the influence of the electrostatic interaction formed by the amine and TiO_2 on the band energy variation of TiO_2. We constructed model systems in which ethylamine molecules were adsorbed on the (110) surface of rutile TiO_2 because modeling an actual polymer/semiconductor interface within the limited unit cell size in DFT simulations is not feasible. On this basis, we can deduce the interaction of amine groups in the PEIE molecule with TiO_2. The atomic geometries of the optimized slab models with ethylamine molecules are shown in Figure 4a and Figure S10. The oxygen atoms attracted electrons and formed a partial negative charge ($\delta-$) after amine groups in ethylamine molecules were bonded to oxygen atoms on TiO_2(110); however, a partial positive charge ($\delta+$) formed at the amine groups. This electron transfer from nitrogen to oxygen well explains the origin of the shift in the N and O 1s peaks, as shown in the XPS data (Figure 3b,c). As a result, a surface dipole was created, and the absolute electronic band energy ionization potential (IP) and electron affinity (EA) were shifted. Figure 4b shows a plot of the calculated IP and EA of bare TiO_2(110) and TiO_2(110) with ethylamine adsorbates. The calculated IP and EA match well with previously reported values.[42] An upward shift of band energies of 0.42 eV was calculated after all oxygen atoms on TiO_2(110) were covered by ethylamine molecules in a 1:1 ratio. The degree of band level shift was mitigated in the case of a 2:1 ratio, where the interaction of half of the oxygen atoms with ethylamine molecules occurs on the TiO_2(110) surface. The magnitude of the calculated band shift is not directly comparable to the UPS result due to the complexity of the real system, where amine groups in the PEIE film also interact with p-Si. However, the upward shift of the band edge coincides with the UPS result of p-Si/PEIE/TiO_2 (10 nm) (Figure 3d). Nonetheless, our DFT calculation results confirm that amine groups establish an electrostatic interaction with TiO_2, inducing an upward shift of TiO_2 band energy level due to the enhanced magnitude of electrostatic interaction.

The magnitude of band bending of PEIE-modified p-Si photocathode was determined via a Mott−Schottky analysis based on an electrochemical impedance spectroscopy (EIS) measurement.[43] The data were fitted according to a Voight equivalent circuit model that has been widely adopted in multilayered photoelectrodes (Figure S11a).[44−46] The p-type doping property of p-Si was observed from the linear line with a negative slope at various applied potentials (Figure 4c). The calculated doping density of the p-Si reaches close to the values suggested by the manufacturer ($\sim 1.32 \times 10^{15}-1.47 \times 10^{16}$) and previous reports (Table S2).[20,46] The Mott−Schottky plot for TiO_2 yields an n-type doping property that could form a p−n junction with p-Si (Figure S11b). The E_{FB} value of the PEIE-modified p-Si photocathode was increased from 0.33 to 0.56 V_{RHE} up to a TiO_2 thickness of 50 nm. However, p-Si/PEIE/TiO_2(70 nm) showed an E_{FB} value nearly identical with that of p-Si/PEIE/TiO_2 (50 nm), which indicates that the band bending of PEIE-modified p-Si photocathode is enhanced with an increasing TiO_2 thickness and reaches a maximum at a thickness of 50 nm. This correlates well with the increased onset potential when the TiO_2 thickness is increased to 50 nm in LSV curves (Figure 2a). Although theoretically the flat band potential estimated using a Mott−Schottky analysis and the photocurrent onset potential as well as the OCP should be similar, due to the presence of interface defects resulting in Fermi level pinning, a slight deviation could appear between the OCP and the flat band potential or the OCP and the onset potential. We may assume PEIE dipole reorientation to be saturated and the band bending to reach its maximum. A TiO_2 layer thicker than 50 nm would act as the series resistance of the device, leading to a decrease in the performance. Our observation in this regard clearly suggests that 50 nm of a TiO_2 overlayer would be a proper thickness when the p-Si photocathode is modified with PEIE. Band diagrams of p-Si/PEIE/TiO_2(∼10 nm) as well as p-Si/PEIE/TiO_2 (∼50 nm) were prepared on the basis of a combination of theoretical calculations and experimental observations (Figure S12). The magnitude of the electrostatic interaction depending on the TiO_2 thickness is described as the band shifting of the TiO_2 layer, resulting in an increased difference in Fermi level between p-Si and TiO_2. This increasing difference causes a large built-in potential to be developed

https://doi.org/10.1021/acsenergylett.2c00392
ACS Energy Lett. 2022, 7, 1392−1402

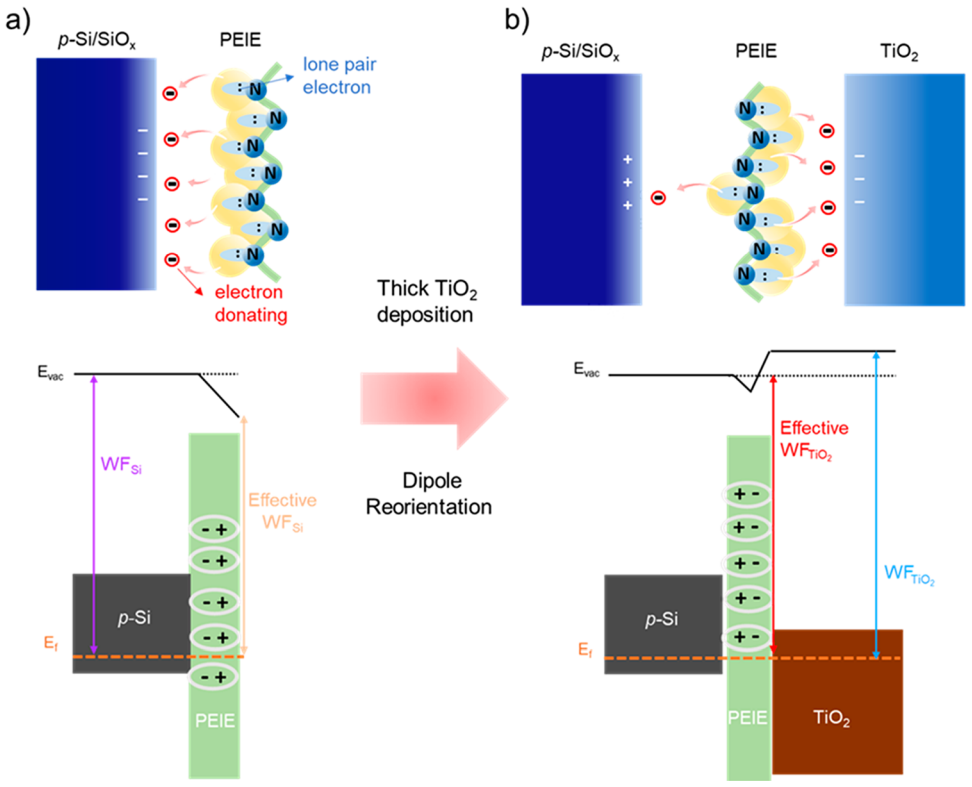

Figure 5. Schematic illustration showing the proposed dipole reorientation mechanism and energy level diagram of PEIE on p-Si (a) before and (b) after thick TiO_2 deposition.

between p-Si and TiO_2, leading to an enhanced band bending and photovoltage.

We measured the performance by varying the PEIE solution concentrations (i.e., 0.01, 0.025, 0.05, 0.1, and 1 wt %) to further confirm the dipole effect based on PEIE thickness (Figure S13a). According to the Mott−Schottky result in Figure 4c, an optimal 50 nm thick TiO_2 was deposited on top of the PEIE-modified p-Si photocathode. The onset potential increased from 0.38 V_{RHE} (0.01 wt % PEIE) to 0.50 V_{RHE} (0.025 wt % PEIE). However, the onset potential decreased to 0.22 V_{RHE} with a further increment of 0.05 wt % in the concentration of PEIE. The current density for the p-Si/PEIE(0.01 wt %)/TiO_2/Pt was 26 mA cm^{-2} at 0 V_{RHE}. The p-Si/PEIE(0.025 wt %)/TiO_2/Pt showed a slightly increased current density (28 mA cm^{-2} at 0 V_{RHE}), whereas p-Si/PEIE(0.05 wt %)/TiO_2/Pt revealed an abrupt decrease in the current density to 5 mA cm^{-2}. No further current was monitored under the condition of 1 wt % PEIE. Furthermore, the statistics of the onset potential obtained from an individual LSV curve for separately fabricating 10 samples at concentrations of 0.01, 0.025, and 0.05 wt % PEIE were obtained to prove the reliability of LSV results depending on PEIE concentration (Figure S13b). Linear extrapolation at 1 mA cm^{-2} could not be performed to define the onset potential, because both 0.1 and 1 wt % PEIE concentrations revealed an inferior current density of less than 1 mA cm^{-2}. Average onset potentials of 0.34 and 0.48 V_{RHE} were obtained from 0.01 and 0.025 wt % PEIE concentrations, respectively; however, 0.16 V_{RHE} was observed for a p-Si photocathode based on 0.05 wt % PEIE deposition. These results imply that PEIE solution deposition enables a highly reproducible and reliable interface modification regardless of its concentration. The PEIE layer thickness as a function of the polymer solution concentration was estimated using ellipsometry (Figure S14). It was observed that the thicker PEIE layer behaves as the series resistance of the photocathode, resulting in suppressing charge transport for a PEIE concentration of greater than 0.05 wt % (~1.4 nm). The photoelectrons are unlikely to tunnel through the thick PEIE layer due to the large band gap energy (6.2 eV) of PEIE, leading it to have an insulating property.[24] At the 0.01 wt % PEIE concentration, the average onset potential had a lower value of 0.34 V_{RHE} in comparison to that for the 0.025 wt % PEIE concentration. It can be inferred that the surface coverage of PEIE deposited at the concentration of 0.01 wt % may be incomplete; hence, the developed dipole magnitude is smaller than that of p-Si/PEIE(0.025 wt %)/TiO_2/Pt. In this regard, the PEIE deposition at a concentration of 0.025 wt % allows an optimal ultrathin layer (~0.5 nm) on top of the p-Si PEC device. Furthermore, we evaluated the morphology of the dipole layer on the Si wafer as a function of the PEIE concentration by AFM (Figure S15). Below the optimum concentration of PEIE (0.025 wt %), there were insignificant changes in the topography and surface roughness in comparison to a bare silicon wafer. However, at a PEIE concentration of 0.05 wt %, we found occasional clusters on the surface. As the concentration increased, these clusters appeared to be agglomerated while the roughness (R_{rms}) sharply increased. On the basis of the AFM results, the PEIE dipole layer seems to be deposited in the form of clusters. However, at a low concentration (under 0.025 wt %), the clusters were hardly observed and PEIE appeared to be deposited conformally. Additionally, we verified the stability of a PEIE-modified planar p-Si photocathode at 0.2 V_{RHE} in an acidic electrolyte of pH 1 under continuous illumination (Figure S16). In the low applied potential region (0.2 V_{RHE}), the PEIE-modified device exhibited a higher current density in

https://doi.org/10.1021/acsenergylett.2c00392
ACS Energy Lett. 2022, 7, 1392−1402

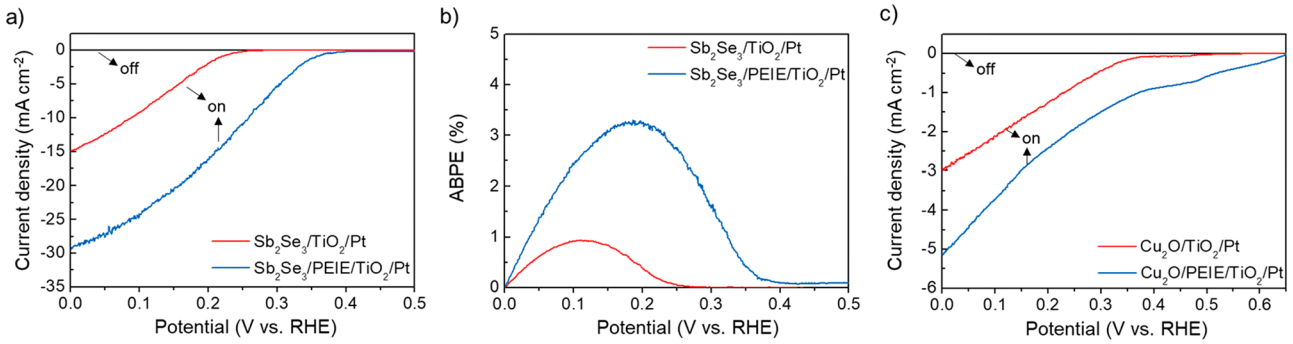

Figure 6. (a) LSV curves and (b) ABPE values of $Sb_2Se_3/TiO_2/Pt$ (red) and $Sb_2Se_3/PEIE/TiO_2/Pt$ (blue) under 1 sun illumination in an H_2SO_4 electrolyte (pH 1). (c) LSV curves of $Cu_2O/TiO_2/Pt$ (red) and $Cu_2O/PEIE/TiO_2/Pt$ (blue) under 1 sun illumination in 1 M KPi (pH 7).

comparison to the p-Si/TiO_2/Pt sample (Figure 2d). Detachment of the Pt cocatalyst from the TiO_2 protective layer has frequently been observed in previous studies.[47,48] To prevent Pt detachment, we deposited a thin TiO_2 (2 nm) layer over the Pt cocatalyst. The PEIE-modified device retained ~80% of its initial current density after 12 h of operation. Under the stable operation of a PEIE-modified device, gas chromatography was used to confirm the amount of photoelectrochemically produced H_2 gas without any side reaction. The quantity of H_2 gas matched well with theoretically calculated H_2 amount, revealing a Faradaic efficiency within a range of 90−100% (Figure S17).

The low onset potential poses an obstacle for operating tandem devices with a p-Si photocathode because of the low band gap of Si, inevitably leading to generation of a small photovoltage. Effective n^+ doping and advanced surface nanostructuring have typically been performed to overcome this limitation by improving the onset potential over 0.5 V_{RHE}.[49,50] However, both approaches involve complicated and expensive processes.[13] Figure S18 shows the previously reported onset potential versus the maximum value of the applied bias photon to current efficiency (ABPE) calculated by excluding a homojunction (surface n^+ doping) or advanced nanostructured p-Si photocathodes or both. Figure S18 shows that there have been several studies of planar p-Si photocathodes, revealing a greatly enhanced onset potential of close to 0.5 V_{RHE}. Among the various strategies, TiO_2 reduction engineering achieved the highest ABPE value (5.9%) with an onset potential of 0.48 V_{RHE}.[51] However, the reduction process involves annealing under an H_2 atmosphere and photoelectrochemical reduction. In contrast, our dipole reorientation strategy can present a facile solution process to enhance the onset potential up to 0.5 V_{RHE} as well as the ABPE value (5.1%). A uniform dipole layer can be achieved through a facile solution deposition, resulting in highly steady and reproducible results. There have been only a few reports on the dramatic improvement of onset potential with high reproducibility via a simple solution process.

The PEIE dipole reorientation before and after thick TiO_2 deposition is schematically depicted in Figure 5. PEIE is an amine-rich polymer capable of donating an electron to the neighboring surface and developing partially positive charges on the polymer, creating a net interfacial dipole between the adsorbent (i.e., p-Si) and adsorbate.[25,52] ALD-derived TiO_2 has a dielectric constant of approximately 47, which is larger than those of Si (11.7) and SiO_2 (3.9).[53] Additionally, it has been reported that the dielectric constant and polarization property of TiO_2 increases as a function of its thickness for all of the values under 70 nm.[54,55] Since the polarizability is responsible for the dielectric constant of the material, when a TiO_2 overlayer having high polarizability is brought into contact with PEIE, the amine-rich polymer preferentially interacts with adjacent TiO_2 by attracting amine groups, resulting in a net dipole reorientation. On consideration of the amine-rich molecular structure of PEIE, hydrogen bonding is highly expected to form between PEIE and SiO_2 or PEIE and TiO_2. Since the dielectric constant of TiO_2 is much higher than that of SiO_2,[53] it can be assumed that stronger hydrogen bonds (dipole interactions) would form between PEIE and TiO_2 in comparison to those between PEIE and SiO_2 due to the higher polarizability of TiO_2 in comparison to SiO_2. Therefore, PEIE can interact more strongly with TiO_2 than with p-Si, developing a large net dipole moment with an increase in TiO_2 thickness. Therefore, a negative charge was strongly induced on the TiO_2 surface, shifting the TiO_2 band edge upward with the increasing TiO_2 thickness; it leads to large band bending with respect to p-Si (Figure 5). The conventional dipole strategies merely control the surface coverage of the dipole layer by varying its concentration; however, our approach can modulate the dipole orientation by the thickness of the TiO_2 overlayer.

Three representative thin-film semiconductors, such Sb_2Se_3, Cu_2O, and SnS, were selected as promising photocathode materials to demonstrate the application versatility of the PEIE diploe reorientation strategy. While the solution-processed Sb_2Se_3 has been proven to serve as an attractive absorber for PEC water splitting, it suffers from a low onset potential even when it has a heterojunction with TiO_2. The decoration of Sb_2Se_3 with PEIE followed by deposition of 30 nm thick ALD TiO_2 and Pt raised the onset potential of Sb_2Se_3 by 0.15 V in comparison to that of the $Sb_2Se_3/TiO_2/Pt$ sample accompanies by a photocurrent density enhancement from 16 to 28 mA cm^{-2}.[56] This observation demonstrates the best performance reported so far in the literature without involvement of a vacuum process (Figure 6a), in which a high ABPE value of 3.3% was observed (Figure 6b).[7,56,57]

We also deposited PEIE on the electrodeposited Cu_2O by spin coating prior to depositing 50 nm thick ALD TiO_2 and Pt. Similarly, the Cu_2O sample modified with PEIE showed an increase of 0.3 V in onset potential in comparison to the $Cu_2O/TiO_2/Pt$ sample without a PEIE modification (Figure 6c). The best onset potential of the $Cu_2O/TiO_2/Pt$ was reported to be approximately 0.4 V_{RHE} at pH 7, while PEIE-modified $Cu_2O/TiO_2/Pt$ showed a record-high onset potential

https://doi.org/10.1021/acsenergylett.2c00392
ACS Energy Lett. 2022, 7, 1392−1402

(i.e., 0.65 V_{RHE} at pH 7) without an additional buffer layer. Furthermore, we additionally demonstrated our concept on the state of the art samples (i.e., pn-Si/TiO_2/Pt, Cu_2O/Ga_2O_3/TiO_2/Pt, SnS/CdS/TiO_2/Pt, and Sb_2Se_3/CdS/TiO_2/Pt photocathodes) (Figure S19). It can be observed that the PEIE dipole effect is limited between an n-type buffer layer and an n-type TiO_2 interlayer. Although the fill factor and performance were slightly enhanced, the onset potential improvement was negligible for other state of the art photocathodes involving already formed p−n junction. As a result, we can conclude that the PEIE dipole effect can significantly develop between a p-type absorber and a highly polarizable n-type semiconductor such as TiO_2.

These observations clearly suggest that our PEIE dipole reorientation strategy has been successfully applied to three representative solution-processed thin-film absorbers that have a heterojunction with TiO_2. Generally, the magnitude of the band shift depends on the amounts of charges that are developed at the interface by the dipole molecules.[16,18] The induced charge density on the surface is related to the polarizability, which can be determined by the dielectric constant.[25] The conventional dipole strategies only focus on modulating the band energy of the p-type absorber layer by positive dipole molecules. However, the magnitude of a band shift by a dipole layer is less effective than modulating the band energy of TiO_2 using a negative dipole because the dielectric constants of absorber layers, such as p-Si, Cu_2O, and Sb_2Se_3, are much smaller than that of ALD TiO_2. Except for p-Si, other polycrystalline semiconductors, such as Cu_2O, SnS, and Sb_2Se_3, suffer from severe surface states and roughness; therefore, they only showed a slight onset potential improvement via the conventional dipole strategy.[7] It has been reported that the roughness and surface state reduce the polarizability or shorten the length of the charge rearrangement induced on the surface.[58,59] Hence, a weak dipole is formed in polycrystalline semiconductors, such as Cu_2O, SnS, and Sb_2Se_3. Therefore, their dipole effect is possibly negligible. In the dipole reorientation strategy of modulating the band edge of TiO_2, in contrast, the negative dipole is well induced on the surface of TiO_2 due to its high polarizability, and the polarizability of TiO_2 increases until its thickness reaches ∼50 nm, resulting in more negative dipoles. Therefore, we conclude that the PEIE dipole reorientation strategy induces larger band bending between the absorber layer and TiO_2 in comparison to the conventional dipole strategy while it is accompanied by a consistent onset potential improvement regardless of the absorber type. However, different degrees of onset potential improvement were observed depending on the absorber types. It is believed that the greater polarizability (i.e., dielectric constant) difference with TiO_2 has a greater PEIE dipole effect. The PEIE dipole reorientation strategy clearly demonstrated an onset potential improvement for TiO_2-protected heterojunction p-type photocathodes with absorber-independent versatility in comparison to previously reported interface engineering.

In summary, we have applied a dipole reorientation strategy, which significantly improves the onset potential of TiO_2-protected p-Si photocathodes, by inserting a PEIE dipole layer into the interface between Si and TiO_2. When a TiO_2 overlayer with high polarizability is brought into contact with PEIE, the amine-rich polymer preferentially interacts with adjacent TiO_2 by attracting amine groups, resulting in a net dipole reorientation. This dipole reorientation becomes saturated when the TiO_2 thickness reaches ∼50 nm. As a result, a negative dipole was strongly induced on the TiO_2 surface, leading to an upward shift in the band edge of the TiO_2-protection layer and enlarged band bending with respect to p-Si. The photovoltage was highly enhanced, and the onset potential was increased to 0.5 V_{RHE} in the p-Si/PEIE/TiO_2/Pt device by controlling the TiO_2-thickness-dependent dipole effect. Our results represent the best onset potential development in comparison to other planar p-Si photocathodes. Furthermore, we successfully transferred the strategy to other p-type absorbers, such as Sb_2Se_3, SnS, and Cu_2O, resulting in an onset potential improvement of at least 0.15 V. This PEIE dipole interlayer method is easily processable, highly reproducible, and universally applicable to diverse TiO_2-protected heterojunction photocathodes, which should be recognized as a noticeable achievement. We believe that our PEIE dipole reorientation strategy can provide a new benchmark to improve the photovoltage of TiO_2-protected heterojunction p-type photocathodes for PEC water splitting.

■ ASSOCIATED CONTENT

Supporting Information

The Supporting Information is available free of charge at https://pubs.acs.org/doi/10.1021/acsenergylett.2c00392.

Experimental procedure. AFM surface topography and XRD patterns of p-Si wafer and p-Si/PEIE. SEM image of PEIE/TiO_2. OCP in the dark with different purging gases, LSV curves of p-Si/PEIE/TiO_2/Pt depending on PEIE concentration, XPS and UPS results of p-Si and bare TiO_2, stability and gas chromatography of the p-Si photocathode, scheme of the band diagram and comparison performance chart of heterojunction p-Si photocathodes, and LSV curves of other state of the art photocathodes (*pn*-Si, Cu_2O/Ga_2O_3, Sb_2Se_3/CdS and SnS/CdS). (PDF)

■ AUTHOR INFORMATION

Corresponding Authors

Aron Walsh − *Department of Materials Science and Engineering, Yonsei University, Seoul 03722, Republic of Korea; Department of Materials, Imperial College London, London SW7 2AZ, U.K.;* orcid.org/0000-0001-5460-7033; Email: a.walsh@imperial.ac.uk

Jooho Moon − *Department of Materials Science and Engineering, Yonsei University, Seoul 03722, Republic of Korea;* orcid.org/0000-0002-6685-9999; Email: jmoon@yonsei.ac.kr

Authors

Juwon Yun − *Department of Materials Science and Engineering, Yonsei University, Seoul 03722, Republic of Korea*

Jeiwan Tan − *Department of Materials Science and Engineering, Yonsei University, Seoul 03722, Republic of Korea*

Young-Kwang Jung − *Department of Materials Science and Engineering, Yonsei University, Seoul 03722, Republic of Korea;* orcid.org/0000-0003-3848-8163

Wooseok Yang − *School of Chemical Engineering, Sungkyunkwan University, Suwon 16419, Korea*

Hyungsoo Lee − *Department of Materials Science and Engineering, Yonsei University, Seoul 03722, Republic of Korea*
Sunihl Ma − *Department of Materials Science and Engineering, Yonsei University, Seoul 03722, Republic of Korea*
Young Sun Park − *Department of Materials Science and Engineering, Yonsei University, Seoul 03722, Republic of Korea*
Chan Uk Lee − *Department of Materials Science and Engineering, Yonsei University, Seoul 03722, Republic of Korea*
Wenzhe Niu − *Department of Chemistry, University of Zurich, Zurich 8057, Switzerland;* orcid.org/0000-0003-1337-8283
Jeongyoub Lee − *Department of Materials Science and Engineering, Yonsei University, Seoul 03722, Republic of Korea*
Kyungmin Kim − *Department of Materials Science and Engineering, Yonsei University, Seoul 03722, Republic of Korea*
S. David Tilley − *Department of Chemistry, University of Zurich, Zurich 8057, Switzerland;* orcid.org/0000-0002-7542-1147

Complete contact information is available at: https://pubs.acs.org/10.1021/acsenergylett.2c00392

Notes

The authors declare no competing financial interest.

■ ACKNOWLEDGMENTS

This research was supported by the National R&D Program through the National Research Foundation of Korea (NRF), funded by the Ministry of Science and ICT (No. 2021R1A3B1068920 and 2021M3H4A1A03049662). This research was also supported by the Yonsei Signature Research Cluster Program of 2021 (2021-22-0002).

■ REFERENCES

(1) Gratzel, M. Photoelectrochemical Cells. *Nature* **2001**, *414*, 338−344.
(2) Sivula, K.; van de Krol, R. Semiconducting Materials for Photoelectrochemical Energy Conversion. *Nat. Rev. Mater.* **2016**, *1*, 15010.
(3) Tan, J.; Yang, W.; Lee, H.; Park, J.; Kim, K.; Hutter, O. S.; Phillips, L. J.; Shim, S.; Yun, J.; Park, Y.; et al. Surface Restoration of Polycrystalline Sb_2Se_3 Thin Films by Conjugated Molecules Enabling High-Performance Photocathodes for Photoelectrochemical Water Splitting. *Appl. Catal., B* **2021**, *286*, 119890.
(4) Yang, W.; Prabhakar, R. R.; Tan, J.; Tilley, S. D.; Moon, J. Strategies for Enhancing the Photocurrent, Photovoltage, and Stability of Photoelectrodes for Photoelectrochemical Water Splitting. *Chem. Soc. Rev.* **2019**, *48*, 4979−5015.
(5) Huang, Q.; Ye, Z.; Xiao, X. D. Recent Progress in Photocathodes for Hydrogen Evolution. *J. Mater. Chem. A* **2015**, *3*, 15824−15837.
(6) Bae, D.; Seger, B.; Vesborg, P. C. K.; Hansen, O.; Chorkendorff, I. Strategies for Stable Water Splitting via Protected Photoelectrodes. *Chem. Soc. Rev.* **2017**, *46*, 1933−1954.
(7) Wick-Joliat, R.; Musso, T.; Prabhakar, R. R.; Lockinger, J.; Siol, S.; Cui, W.; Severy, L.; Moehl, T.; Suh, J.; Hutter, J.; et al. Stable and Tunable Phosphonic Acid Dipole Layer for Band Edge Engineering of Photoelectrochemical and Photovoltaic Heterojunction Devices. *Energ Environ. Sci.* **2019**, *12*, 1901−1909.
(8) Park, J.; Yang, W.; Oh, Y.; Tan, J.; Lee, H.; Boppella, R.; Moon, J. Efficient Solar-to-Hydrogen Conversion from Neutral Electrolytes Using Morphology-Controlled Sb_2Se_3 Light Absorbers. *ACS Energy Lett.* **2019**, *4*, 517−526.
(9) Li, C. L.; Hisatomi, T.; Watanabe, O.; Nakabayashi, M.; Shibata, N.; Domen, K.; Delaunay, J.-J. Positive Onset Potential and Stability of Cu_2O-based Photocathodes in Water Splitting by Atomic Layer Deposition of a Ga_2O_3 Buffer Layer. *Energ Environ. Sci.* **2015**, *8*, 1493−1500.
(10) Lee, H.; Yang, W.; Tan, J.; Park, J.; Shim, S. G.; Park, Y. S.; Yun, J. W.; Kim, K. M.; Moon, J. High-Performance Phase-Pure SnS Photocathodes for Photoelectrochemical Water Splitting Obtained via Molecular Ink-Derived Seed-Assisted Growth of Nanoplates. *ACS Appl. Mater. Interfaces.* **2020**, *12*, 15155−15166.
(11) Kuang, Y.; Yamada, T.; Domen, K. Surface and Interface Engineering for Photoelectrochemical Water Oxidation. *Joule* **2017**, *1*, 290−305.
(12) Boettcher, S. W.; Warren, E. L.; Putnam, M. C.; Santori, E. A.; Turner-Evans, D.; Kelzenberg, M. D.; Walter, M. G.; McKone, J. R.; Brunschwig, B. S.; Atwater, H. A.; et al. Photoelectrochemical Hydrogen Evolution Using Si Microwire Arrays. *J. Am. Chem. Soc.* **2011**, *133*, 1216−1219.
(13) Li, H.; Liu, B.; Feng, S. J.; Li, H.; Wang, T.; Gong, J. Construction of Uniform Buried pn Junctions on Pyramid Si Photocathodes Using a Facile and Safe Spin-on Method for Photoelectrochemical Water Splitting. *J. Mater. Chem. A* **2020**, *8*, 224−230.
(14) Seger, B.; Laursen, A. B.; Vesborg, P. C. K.; Pedersen, T.; Hansen, O.; Dahl, S.; Chorkendorff, I. Hydrogen Production Using a Molybdenum Sulfide Catalyst on a Titanium-Protected n plus p-Silicon Photocathode. *Angew. Chem., Int. Ed.* **2012**, *51*, 9128−9131.
(15) Yang, W.; Kim, J. H.; Hutter, O. S.; Phillips, L. J.; Tan, J.; Park, J.; Lee, H.; Major, J. D.; Lee, J. S.; Moon, J. Benchmark Performance of Low-Cost Sb_2Se_3 Photocathodes for Unassisted Solar Overall Water Splitting. *Nat. Commun.* **2020**, *11*, 861.
(16) Chen, Q.; Wang, C.; Li, Y.; Chen, L. Interfacial Dipole in Organic and Perovskite Solar Cells. *J. Am. Chem. Soc.* **2020**, *142*, 18281−18292.
(17) Canil, L.; Cramer, T.; Fraboni, B.; Ricciarelli, D.; Meggiolaro, D.; Singh, A.; Liu, M. N.; Rusu, M.; Wolff, C. M.; Phung, N.; et al. Tuning Halide Perovskite Energy Levels. *Energ Environ. Sci.* **2021**, *14*, 1429−1438.
(18) Guijarro, N.; Prevot, M. S.; Sivula, K. Surface Modification of Semiconductor Photoelectrodes. *Phys. Chem. Chem. Phys.* **2015**, *17*, 15655−15674.
(19) Boucher, D. G.; Kearney, K.; Ertekin, E.; Rose, M. J. Tuning p-Si(111) Photovoltage via Molecule|Semiconductor Electronic Coupling. *J. Am. Chem. Soc.* **2021**, *143*, 2567−2580.
(20) Seo, J.; Kim, H. J.; Pekarek, R. T.; Rose, M. J. Hybrid Organic/Inorganic Band-Edge Modulation of p-Si(111) Photoelectrodes: Effects of R, Metal Oxide, and Pt on H_2 Generation. *J. Am. Chem. Soc.* **2015**, *137*, 3173−3176.
(21) MacLeod, B. A.; Steirer, K. X.; Young, J. L.; Koldemir, U.; Sellinger, A.; Turner, J. A.; Deutsch, T. G.; Olson, D. C. Phosphonic Acid Modification of $GaInP_2$ Photocathodes Toward Unbiased Photoelectrochemical Water Splitting. *ACS Appl. Mater. Interfaces* **2015**, *7*, 11346−11350.
(22) Kim, S. Y.; Lee, J.-L. Effect of Interfacial Layer Thickness on the Formation of Interface Dipole in Metal/Tris(8-hydroxyquinoline) Aluminum Interface. *Org. Electron.* **2008**, *9*, 678−686.
(23) Kim, S. Y.; Hong, K.; Lee, J.-L. Change of Interface Dipole Energy with Interfacial Layer Thickness and O_2 Plasma Treatment in Metal/Organic Interface. *Appl. Phys. Lett.* **2007**, *90*, 183508.
(24) Zhou, Y.; Fuentes-Hernandez, C.; Shim, J.; Meyer, J.; Giordano, A. J.; Li, H.; Winget, P.; Papadopoulos, T.; Cheun, H.; Kim, J.; et al. A Universal Method to Produce Low-Work Function Electrodes for Organic Electronics. *Science* **2012**, *336*, 327−332.
(25) Vilan, A.; Cahen, D. Chemical Modification of Semiconductor Surfaces for Molecular Electronics. *Chem. Rev.* **2017**, *117*, 4624−4666.

(26) Ha, J.; Kim, H.; Lee, H.; Lim, K. G.; Lee, T. W.; Yoo, S. Device Architecture for Efficient, Low-Hysteresis Flexible Perovskite Solar Cells:. Replacing TiO_2 with C_{60} Assisted by Polyethylenimine Ethoxylated Interfacial Layers. *Sol. Energy Mater. Sol. C* **2017**, *161*, 338−346.
(27) Crespo-Quesada, M.; Pazos-Outon, L. M.; Warnan, J.; Kuehnel, M. F.; Friend, R. H.; Reisner, E. Metal-encapsulated Organolead Halide Perovskite Photocathode for Solar-Driven Hydrogen Evolution in Water. *Nat. Commun.* **2016**, *7*, 12555.
(28) Song, S.; Moon, B. J.; Horantner, M. T.; Lim, J.; Kang, G.; Park, M.; Kim, J. Y.; Snaith, H. J.; Park, T. Interfacial electron accumulation for efficient homo-junction perovskite solar cells. *Nano Energy* **2016**, *28*, 269−276.
(29) Gleason-Rohrer, D. C.; Brunschwig, B. S.; Lewis, N. S. Measurement of the Band Bending and Surface Dipole at Chemically Functionalized Si(111)/Vacuum Interfaces. *J. Phys. Chem. C* **2013**, *117*, 18031−18042.
(30) Zhong, M.; Hisatomi, T.; Kuang, Y. B.; Zhao, J.; Liu, M.; Iwase, A.; Jia, Q. X.; Nishiyama, H.; Minegishi, T.; Nakabayashi, M.; et al. Surface Modification of CoO_x Loaded $BiVO_4$ Photoanodes with Ultrathin p-Type NiO Layers for Improved Solar Water Oxidation. *J. Am. Chem. Soc.* **2015**, *137*, 5053−5060.
(31) Ye, K.-H.; Li, H. B.; Huang, D.; Xiao, S.; Qiu, W. T.; Li, M. Y.; Hu, Y. W.; Mai, W. J.; Ji, H. B.; Yang, S. H. Enhancing Photoelectrochemical Water Splitting by Combining Work Function Tuning and Heterojunction Engineering. *Nat. Commun.* **2019**, *10*, 3687.
(32) Berglund, S. P.; Abdi, F. F.; Bogdanoff, P.; Chernseddine, A.; Friedrich, D.; van de Krol, R. Comprehensive Evaluation of $CuBi_2O_4$ as a Photocathode Material for Photoelectrochemical Water Splitting. *Chem. Mater.* **2016**, *28*, 4231−4242.
(33) Olivieri, G.; Cossaro, A.; Capria, E.; Benevoli, L.; Coreno, M.; De Simone, M.; Prince, K. C.; Kladnik, G.; Cvetko, D.; Fraboni, B.; et al. Intermolecular Hydrogen Bonding and Molecular Orbital Distortion in 4-Hydroxycyanobenzene Investigated by X-ray Spectroscopy. *J. Phys. Chem. C* **2015**, *119*, 121−129.
(34) Hsu, J.-C.; Lin, Y.-H.; Wang, P. W. X-ray Photoelectron Spectroscopy Analysis of Nitrogen-Doped TiO_2 Films Prepared by Reactive-Ion-Beam Sputtering with Various NH_3/O_2 Gas Mixture Ratios. *Coatings* **2020**, *10*, 47.
(35) Ma, H.-P.; Lu, H.-L.; Yang, J.-H.; Li, X.-X.; Wang, T.; Huang, W.; Yuan, G.-J.; Komarov, F. F.; Zhang, D. W. Measurements of Microstructural, Chemical, Optical, and Electrical Properties of Silicon-Oxygen-Nitrogen Films Prepared by Plasma-Enhanced Atomic Layer Deposition. *Nanomaterials* **2018**, *8*, 1008.
(36) Pisarek, M.; Krawczyk, M.; Holdynski, M.; Lisowski, W. Plasma Nitriding of TiO_2 Nanotubes: N-Doping in Situ Investigations Using XPS. *ACS Omega* **2020**, *5*, 8647−8658.
(37) Ji, T.; Liu, Q.; Zou, R.; Zhang, Y.; Wang, L.; Sang, L.; Liao, M.; Hu, J. Enhanced UV-Visible Light Photodetectors with a TiO_2/Si Heterojunction Using Band Engineering. *J. Mater. Chem. C* **2017**, *5*, 12848−12856.
(38) Gupta, P.; Soni, M.; Sharma, S. K. Alternate Lanthanum Oxide/Silicon Oxynitride-Based Gate Stack Performance Enhancement Due to Ultrathin Oxynitride Interfacial Layer for CMOS Applications. *J. Mater. Sci.: Mater. Electron.* **2020**, *31*, 1986−1995.
(39) Yang, X.; Ying, Z.; Yang, Z.; Xu, J- R.; Wang, W.; Wang, J.; Wang, Z.; Yao, L.; Yan, B.; Ye, J. Light-Promoted Electrostatic Adsorption of High-Density Lewis Base Monolayers as Passivating Electron-Selective Contacts. *Adv. Sci.* **2021**, *8*, 2003245.
(40) Lee, J.-H.; Kim, J.; Kim, G.; Shin, D.; Jeong, S. Y.; Lee, J.; Hong, S.; Choi, J. W.; Lee, C.-L.; Kim, H.; et al. Introducing Paired Electric Dipole Layers for Efficient and Reproducible Perovskite Solar Cells. *Energ Environ. Sci.* **2018**, *11*, 1742−1751.
(41) Zhang, H.; Azimi, H.; Hou, Y.; Ameri, T.; Przybilla, T.; Spiecker, E.; Kraft, M.; Scherf, U.; Brabec, C. J. Improved High-Efficiency Perovskite Planar Heterojunction Solar Cells via Incorporation of a Polyelectrolyte Interlayer. *Chem. Mater.* **2014**, *26*, 5190−5193.
(42) Cheng, J.; Sprik, M. Aligning Electronic Energy Levels at the TiO_2/H_2O Interface. *Phys. Rev. B* **2010**, *82*, 081406.
(43) Gelderman, K.; Lee, L.; Donne, S. W. Flat-Band Potential of a Semiconductor: Using the Mott−Schottky Equation. *J. Chem. Educ.* **2007**, *84*, 685.
(44) Sartori, A.; Orlandi, M.; Berardi, S.; Mazzi, A.; Bazzanella, N.; Caramori, S.; Boaretto, R.; Natali, M.; Fernandes, R.; Patel, N.; et al. Functionalized p-silicon Photocathodes for Solar Fuels Applications: Insights from Electrochemical Impedance Spectroscopy. *Electrochim. Acta* **2018**, *271*, 472−480.
(45) Monny, S. A.; Zhang, L.; Wang, Z. L.; Luo, B.; Konarova, M.; Du, A. J.; Wang, L. Z. Fabricating Highly Efficient Heterostructured $CuBi_2O_4$ Photocathodes for Unbiased Water Splitting. *J. Mater. Chem. A* **2020**, *8*, 2498−2504.
(46) Yang, W.; Moehl, T.; Service, E.; Tilley, S. D. Operando Analysis of Semiconductor Junctions in Multi-Layered Photocathodes for Solar Water Splitting by Impedance Spectroscopy. *Adv. Energy Mater.* **2021**, *11*, 2003569.
(47) Paracchino, A.; Laporte, V.; Sivula, K.; Gratzel, M.; Thimsen, E. Highly Active Oxide Photocathode for Photoelectrochemical Water Reduction. *Nat. Mater.* **2011**, *10*, 456−461.
(48) Rojas, H. C.; Bellani, S.; Fumagalli, F.; Tullii, G.; Leonardi, S.; Mayer, M. T.; Schreier, M.; Gratzel, M.; Lanzani, G.; Di Fonzo, F.; et al. Polymer-based Photocathodes with a Solution-Processable Cuprous Iodide Anode Layer and a Polyethyleneimine Protective Coating. *Energ Environ. Sci.* **2016**, *9*, 3710−3723.
(49) Vanka, S.; Arca, E.; Cheng, S.; Sun, K.; Botton, G. A.; Teeter, G.; Mi, Z. High Efficiency Si Photocathode Protected by Multifunctional GaN Nanostructures. *Nano Lett.* **2018**, *18*, 6530−6537.
(50) Fan, R.; Dong, W.; Fang, L.; Zheng, F.; Shen, M. More than 10% Efficiency and One-Week Stability of Si Photocathodes for Water Splitting by Manipulating the Loading of the Pt Catalyst and TiO_2 Protective Layer. *J. Mater. Chem. A* **2017**, *5*, 18744−18751.
(51) Li, H.; Wang, T.; Liu, S.; Luo, Z.; Li, L.; Wang, H.; Zhao, Z.-J.; Gong, J. Controllable Distribution of Oxygen Vacancies in Grain Boundaries of p-Si/TiO_2 Heterojunction Photocathodes for Solar Water Splitting. *Angew. Chem., Int. Ed.* **2021**, *60*, 4034−4037.
(52) Yang, M.; Qin, F.; Wang, W.; Liu, T.; Sun, L.; Xie, C.; Dong, X.; Lu, X.; Zhou, Y. A Metal Chelation Strategy Suppressing Chemical Reduction between PEDOT and Polyethylenimine for a Printable Low-Work Function Electrode in Organic Solar Cells. *J. Mater. Chem. A* **2021**, *9*, 3918−3924.
(53) Wei, D.; Hossain, T.; Garces, N. Y.; Nepal, N.; Meyer, H. M.; Kirkham, M. J.; Eddy, C. R.; Edgar, J. H. Influence of Atomic Layer Deposition Temperatures on TiO_2/n-Si MOS Capacitor. *ECS J. Solid State Sci. Technol.* **2013**, *2*, N110.
(54) Elsaeedy, H. I.; Qasem, A.; Yakout, H. A.; Mahmoud, M. The Pivotal Role of TiO_2 Layer Thickness in Optimizing the Performance of TiO_2/p-Si Solar Cell. *J. Alloys Compd.* **2021**, *867*, 159150.
(55) Kim, S. K.; Kim, W.-D.; Kim, K.-M.; Hwang, C. S.; Jeong, J. High Dielectric Constant TiO_2 Thin Films on a Ru Electrode Grown at 250 °C by Atomic-Layer Deposition. *Appl. Phys. Lett.* **2004**, *85*, 4112.
(56) Yang, W.; Ahn, J.; Oh, Y.; Tan, J.; Lee, H.; Park, J.; Kwon, H. C.; Kim, J.; Jo, W.; Kim, J.; et al. Adjusting the Anisotropy of 1D Sb_2Se_3 Nanostructures for Highly Efficient Photoelectrochemical Water Splitting. *Adv. Energy Mater.* **2018**, *8*, 1702888.
(57) Lee, H.; Yang, W.; Tan, J.; Oh, Y.; Park, J.; Moon, J. Cu-Doped NiO_x as an Effective Hole-Selective Layer for a High-Performance Sb_2Se_3 Photocathode for Photoelectrochemical Water Splitting. *ACS Energy Lett.* **2019**, *4*, 995−1003.
(58) Zojer, E.; Taucher, T. C.; Hofmann, O. T. The Impact of Dipolar Layers on the Electronic Properties of Organic/Inorganic Hybrid Interfaces. *Adv. Mater. Interfaces* **2019**, *6*, 1900581.
(59) Sun, X.; Su, Y. J.; Gao, K. W.; Guo, L. Q.; Qiao, L. J. Charge Accumulation in Grain Boundary Promotes Intergranular Fracture of Lead Zirconate Titanate Piezoceramics under Mechanical and Electric Load. *Scr. Mater.* **2012**, *66*, 292.

https://doi.org/10.1021/acsenergylett.2c00392
ACS Energy Lett. 2022, 7, 1392−1402